LoRaAid: Underground Joint Communication and Localization System Based on LoRa Technology

Huaijin Zhang, Guanghua Liu, *Member, IEEE*,
You Xu, *Graduate Student Member, IEEE*, and Tao Jiang, *Fellow, IEEE*

***Abstract*— Much exploration has been conducted to ensure the successful implementation of underground applications based on wireless underground sensor networks (WUSNs). However, most of them only focus on the communication aspect while neglecting location information. As a matter of fact, for scenarios such as earthquake and mine emergency rescue, it is necessary to achieve communication and positioning simultaneously. Nevertheless, accomplishing this goal is challenging, as the underground environment not only causes tremendous attenuation but also has limited hardware resources. Long range (LoRa) technology has high reception sensitivity and a simple structure, making it well suited for underground emergency rescue. Therefore, we propose a LoRa-based joint communication and localization system called LoRaAid. When a disaster occurs, the wearable LoRa device transmits sensing information to surrounding buried nodes. Through collaboration between nodes, diversity reception of signals and location acquisition of the target can be achieved simultaneously. Two different schemes are proposed to achieve correct demodulation, and the closed-form expression for bit error rate (BER) is also derived. While implementing communication, LoRaAid uses the mapping relationship between noise-reduced received signal strength indicator (RSSI) and distance to achieve trilateral localization. Numerous experimental results demonstrate that LoRaAid can enable long-range communication while achieving decimeter-level positioning accuracy.**

***Index Terms*— Wireless underground sensor networks (WUSNs), long range (LoRa), joint communication and localization, spatial diversity, received signal strength indicator (RSSI).**

I. Introduction

WIRELESS underground sensor networks (WUSNs), which consist of multiple buried sensor nodes, have received significant attention in recent years due to their potential for various applications such as precision agriculture [1], real-time structure detection [2], efficient post-earthquake rescue [3], [4], unmanned border patrol [5], and many other underground activities [6]. In this case, a large amount of information, such as location, geology, humidity, and vital signs, needs to be transmitted through the soil. However, the underground environment is intricate due to the heterogeneous nature of the soil, which consists of sand, rock, clay, and plant roots. Therefore, carrying out underground applications is fraught with difficulties and challenges.

A great deal of work has been explored on various aspects to ensure the successful implementation of underground applications in WUSNs, including device deployment [7], [8], channel modeling [9], [10], routing protocols [11], [12], and so on. Despite their impressive achievements, they have mostly concentrated on the study of communication performance while neglecting location information. Especially in emergency rescues such as earthquakes and mine disasters, locating trapped people is as important as communicating with them [7]. In addition, since communication opportunities are extremely limited, it is valuable to use the same receive signal to achieve these two goals simultaneously. Therefore, an integrated communication and localization system is urgently needed for underground rescue scenarios, which not only improves rescue efficiency but also quickly builds a life-saving bridge. However, the design of such a system faces many challenges. Not only does it need to combat the impact of high attenuation on communication performance, but it also has to use lightweight devices that enable positioning with limited hardware resources. Existing underground communication and localization technologies suffer from some degree of problems, such as small communication ranges, expensive and bulky equipment, and the need for alignment between devices, which make them difficult to meet the demand.

To this end, we propose a joint communication and localization system based on Long Range (LoRa) technology, called **LoRaAid**. That is because LoRa has the characteristics of high reception sensitivity and simple structure, making it possible to communicate and locate simultaneously in harsh environments with limited resources [13], [14], [15], [16], [17], [18]. In our considered scenario, LoRa nodes have been deployed in the danger zone and are still operating after a disaster has occurred. The working procedure of LoRaAid is as follows: *a)* Everyone in a building or mine needs to carry a wearable LoRa device, which automatically transmits

Manuscript received 17 April 2023; revised 27 July 2023; accepted 12 October 2023. Date of publication 24 October 2023; date of current version 10 May 2024. This work was supported in part by the National Natural Science Foundation of China under Grant 62001177 and Grant 62371200. The associate editor coordinating the review of this article and approving it for publication was Y. Wu. *(Corresponding author: Guanghua Liu.)*

Huaijin Zhang is with the Research Center of 6G Mobile Communications, School of Cyber Science and Engineering and the School of Electronic Information and Communications, Huazhong University of Science and Technology, Wuhan 430074, China (e-mail: huaijinzhang@hust.edu.cn).

Guanghua Liu and Tao Jiang are with the Research Center of 6G Mobile Communications, School of Cyber Science and Engineering, Huazhong University of Science and Technology, Wuhan 430074, China (e-mail: guanghualiu@hust.edu.cn; tao.jiang@ieee.org).

You Xu is with the Wuhan National Laboratory for Optoelectronics, Research Center of 6G Mobile Communications, School of Cyber Science and Engineering, Huazhong University of Science and Technology, Wuhan 430074, China (e-mail: youxu@hust.edu.cn).

Color versions of one or more figures in this article are available at https://doi.org/10.1109/TWC.2023.3325330.

Digital Object Identifier 10.1109/TWC.2023.3325330

perception information to the surrounding LoRa nodes fixed in the soil. *b)* The surrounding nodes transmit the received signal to the data center for further processing. *c)* Data center combines the received signals from multiple nodes to demodulate the information and calculates the exact location of the target node.

The highlight of the LoRaAid system is that different locations of surrounding nodes can not only provide received signal strength indication (RSSI) information for localization but also form spatial diversity, which can improve the reliability of communication. Even though the signal-to-noise ratio (SNR) may be below the threshold of a single node, it is still possible to achieve correct demodulation by combining signals from multiple nodes to make SNR exceed the threshold [19]. Depending on the limitation of hardware equipment and the requirement of accuracy, two different schemes, maximal ratio combining (MRC) with coherent demodulation or equal-gain combining (EGC) with non-coherent demodulation, can be used to achieve the diversity reception of signals. While implementing communication, the system performs noise reduction on the received signals and utilizes the obtained RSSI to achieve trilateral localization. The main contributions of this paper are summarized as follows.

- To the best of our knowledge, this paper is the first attempt at joint communication and localization using LoRa for underground rescue scenarios. Our proposed system LoRaAid exploits the differences in the spatial location of multiple nodes, improves communication quality through collaboration between multiple nodes, and uses the RSSI of each node for trilateral localization.
- To achieve signal diversity reception, we propose two different schemes, MRC with coherent demodulation and EGC with non-coherent demodulation. A closed-form expression for the BER performance of the LoRa coherent demodulation scheme is derived to demonstrate that multi-node collaboration can extend communication coverage. To obtain the target location, we propose a precise localization algorithm based on noise-reduced RSSI without adding extra overhead.
- We design the prototype of LoRaAid and perform field experiments using hardware devices. Numerous experiments are conducted to investigate the effects of LoRa parameter configuration, noise reduction algorithm, and soil moisture on system performance.
- Experimental results verify that LoRaAid can achieve reliable long-distance communication (over 5 m) and accurate positioning (decimeter-level) under adverse conditions (high soil moisture and high transmission rate).
- We perform a detailed energy consumption calculation and compare LoRaAid with the conventional system. The results show that battery life can be significantly extended with LoRaAid.

The rest of this paper is organized as follows: Section II first reviews the relevant literature. Section III presents the system model of LoRaAid and introduces the fundamental principles of LoRa signal and underground propagation of electromagnetic (EM) waves. Section IV shows the combination method to demodulate the received signal as well as the noise-reduced localization algorithm to find the target. In addition, the performance of LoRaAid in terms of energy consumption is also analyzed. Section V introduces the design and implementation of LoRaAid. Section VI presents the actual experimental results. Section VII concludes the paper.

II. Related Works

Recent years have witnessed great strides in underground communication and localization technologies, and we briefly introduce them as follows.

A. Underground Wireless Communication

Solutions for underground wireless communication consist of acoustic, magnetic induction (MI), visible light (VLC), and EM waves. Acoustic waves are used to detect underground objects and soil moisture, as well as for mine communications [20]. However, acoustic techniques are challenging due to vibration limitations and the influence of acoustic noise along the drill pipe. In MI communication, the signal strength attenuates with the inverse cubic coefficient of distance and high data rate [1], [4], [8], [10]. Moreover, communication is not possible if the coils of the transmitter and receiver are perpendicular to each other. Therefore, MI cannot be easily implemented underground. For the VLC system, it can only be used for oil and gas field monitoring because light cannot pass through the soil [21]. Moreover, the light propagation is affected by gas and requires perfect alignment between the Light-Emitting Diode (LED) and photo-detector, making the application scenarios limited. EM waves are widely used for underground communication and sensing to enable various applications [9], [22], [23]. However, its practical implementation still faces several key challenges, such as energy consumption and high attenuation.

B. LoRa-Based Underground Wireless Communication

LoRa technology has the characteristics of high reception sensitivity and low power consumption, which can effectively improve the quality of EM signal transmission and significantly extend the operation cycle of buried nodes. Therefore, a series of explorations and analyses have been conducted on LoRa-based underground communication. A system for testing LoRa propagation in the soil is presented firstly in [13]. In [14], the transmission performance of LoRa in underground channels is studied theoretically and empirically. Additionally, the relationship between LoRa transmission range and bit-error-rate (BER) is derived based on the statistical underground channel model. The authors of [15] discuss the usability of LoRa and LoRaWAN protocols for underground monitoring activities. The channel models for underground-to-aboveground (UG2AG) and aboveground-to-underground (AG2UG) communication are investigated in [16]. The effects of propagation direction, physical layer parameters, and burial depth on LoRa propagation performance are analyzed experimentally. An adaptive LoRa parameter selection method for UG2AG link quality assessment is proposed in [17]. The proposed environment-aware mechanism can significantly extend

the lifespan of wireless sensor nodes. The authors of [18] develop a model of a non-backfilled channel, and the effects of propagation direction, burial depth, inter-node distance, and backfill conditions on the link quality are experimentally quantified. Existing studies only consider the communication performance of LoRa signals without realizing the urgency of underground node localization. In fact, LoRa has the ability to achieve precise localization while guaranteeing communication performance.

C. Underground Localization

In recent years, underground localization has also received considerable attention. Both radio frequency identification (RFID) and ZigBee have been used to locate miners [24], [25], [26]. However, the propagation distance of RFID is very short in the air medium of a mine, let alone in the complex underground environment with high attenuation where earthquakes and mine collapses occur. In addition, LoRa is over 20dB more sensitive than ZigBee, and the working distance is over ten times farther. Despite the high accuracy of ultra wideband (UWB) measurement, the equipment is expensive and requires a large bandwidth [27]. Visible light positioning (VLP) offers a new approach to underground localization [28], [29], [30], [31]. However, light propagation is affected by gases and requires perfect alignment between the LED and photo-detector, making visible light signal transmission extremely unreliable. Although a few related works have explored MI-based localization [32], [33], [34], it is still not considered a good choice for underground localization. That is because MI localization cannot work if the sender and receiver coils are perpendicular to each other, which is likely to happen when the sensors shift considerably. The common drawback of existing underground localization solutions is that they are unable to communicate over long distances while achieving localization.

While current underground communication and localization solutions can perform well in their own ways, there is still a lack of research to achieve them simultaneously. Considering the limited communication opportunities, it is significant to use only one signal to achieve both without increasing the communication overhead. Therefore, we propose the LoRaAid system for the scenario of rescuing trapped people in a disaster.

III. System Model

Due to the complicated nature of the underground environment, designing a rescue system in WUSNs faces two challenges, *1) severe underground attenuation, which greatly restricts the communication distance between nodes, 2) limited hardware resources and communication opportunities, which require the use of lightweight devices that can perform simultaneous communication and positioning with only one signal.* In order to tackle these two problems, we present the LoRaAid system based on WUSNs.

Considering the high reception sensitivity of LoRa technology and its lightweight device with a simple structure, LoRaAid utilizes LoRa technology to achieve reliable communication and decimeter-level positioning simultaneously. Fig. 1 shows an illustration of the LoRaAid system model. As shown in the figure, a collaborative effort of the nodes can be used to locate people in collapsed buildings and also to improve the reliability of communication. LoRaAid consists of a LoRa transmitter (target) and several LoRa receivers connected to the gateway. We assume that each node is a single-antenna device, (x_i, y_i) is the position of the i-th node, and (x, y) is the unknown position of the target. The number of receiving nodes defined as M should be at least three to achieve localization. For the convenience of analysis, it is set as three receivers in the following content. Here, we consider the case where the receiving nodes are at the same depth as the target, but in the future, we can also extend to the case of different depths.

When a person is trapped, the portable LoRa device will transmit a signal $s_m(nT)$, where $m \in \{0, 1, 2, \ldots, 2^{SF} - 1\}$ represents the transmitted symbol, T is the sampling interval and $n \in \{0, 1, 2, \ldots, 2^{\mathrm{SF}} - 1\}$ depicts the sample index at time nT. SF represents the spreading factor, which is also the number of information bits encoded into one LoRa symbol. After the signal propagates in soil, the i-th node buried in the surroundings will receive the signal $r_i(nT)$. To solve the first challenge, LoRaAid utilizes the concept of spatial diversity. Different locations of nodes lead to different channel coefficients, resulting in spatial diversity, which allows the system to improve LoRa packet reception performance in underground ultra-low SNR scenarios. Even though the SNR may be below the threshold of a single node, we can still realize correct packet demodulation by combining signals from multiple nodes and pulling the SNR above the threshold. To solve the second challenge, LoRaAid uses the RSSI of received LoRa signals to achieve localization. This is because the LoRa terminals have simple architecture, so using RSSI for localization avoids the complex synchronization problem and allows simultaneous communication and localization based on limited hardware resources and communication opportunities. In this case, the distance R_i between the transmitter and the i-th receiver is calculated based on the underground channel model and obtained RSSI. The estimated location region of the transmitter is obtained by the intersection of the circles corresponding to different receiving nodes. Once we establish the localization equations, the coordinate of the transmitter is obtained using the Taylor series expansion algorithm. It is worth noting that the case of nodes located at the same depth that we describe in the article is the most basic two-dimensional localization without loss of generality. Two-dimensional localization requires at least three anchor nodes that are not in the same line, while three-dimensional localization requires at least four anchor nodes that are not in the same plane, but the fundamentals are the same and can easily be extended further.

Based on this, we next provide detailed descriptions of the LoRa transmit signal (in Section III-A), the underground propagation model of LoRaAid (in Section III-B), and the joint communication and localization processing (in Section IV).

A. Transmit Signal in LoRaAid

When a person is trapped, the accompanying LoRa device will transmit LoRa signals to the surrounding area. In the

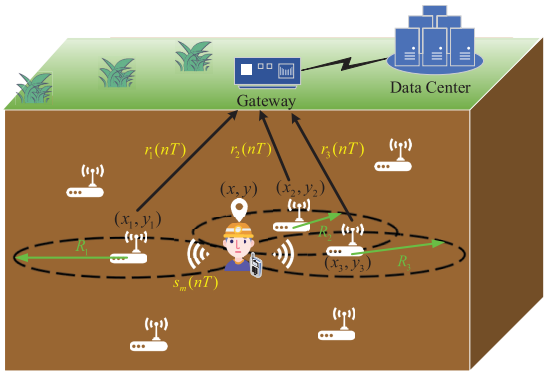

Fig. 1. The illustration diagram of proposed LoRaAid model. When the target node transmits information to its surroundings, several buried nodes closest to the target send the signal back to the data center for signal combination and demodulation, as well as target localization.

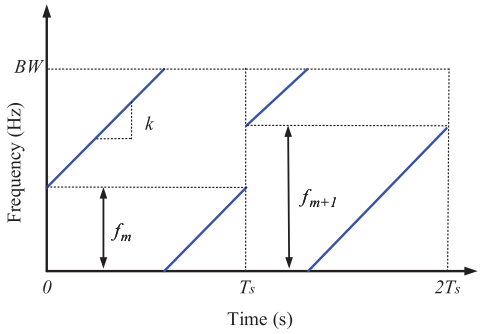

Fig. 2. Spectrogram of LoRa modulation symbols.

following, we describe the characteristics of the transmitted LoRa signal.

LoRa adopts the chirp spread spectrum (CSS) mechanism to encode data. The frequency of a LoRa symbol shifts cyclically over time. LoRa modulation maps every SF bits to a symbol $m \in \{0, 1, 2, \ldots, 2^{SF} - 1\}$. Each LoRa symbol m is characterized by a frequency offset $f_m = \mathrm{BW} \cdot m/2^{\mathrm{SF}}$ that sets the starting frequency of the corresponding chirp signal. BW is the transmission bandwidth. During the symbol duration T_s, the signal frequency corresponding to m increases linearly with a slope of $k = \frac{\mathrm{BW}}{T_s}$ from f_m until it reaches BW. The chirp signal frequency then wraps around 0 before it continues to increase linearly again until the end of T_s. With a sampling rate of $1/T$, the LoRa waveform $s_m(nT)$ corresponding to the LoRa symbol m is composed of 2^{SF} samples, denoted as [35]

$$s_m(nT) = \sqrt{\frac{E_s}{2^{\mathrm{SF}}}} e^{j2\pi \frac{((m+n) \mod 2^{\mathrm{SF}})^2}{2^{\mathrm{SF}+1}}}, \tag{1}$$

where E_s depicts the symbol energy. A spectrogram of two LoRa symbols is shown in Fig. 2.

B. Channel Model in LoRaAid

Since the most obvious feature of the underground compared to the ground is the severe signal attenuation, so we first introduce the large-scale propagation effects of the underground channel. Wherein the most important characteristic is the relationship between received signal strength and distance.

It is well known that the received signal strength P_r in an underground environment is expressed in logarithmic form as

$$P_r(dBm) = P_t(dBm) + G_t(dB) + G_r(dB) - L_{UG}(dB), \tag{2}$$

where P_t is the transmit power, G_t and G_r are the gains of the transmitter and receiver antennas. The path loss L_{UG} can be given as

$$L_{UG} = 6.4 + 20\log(R) + 20\log(\beta) + 8.69\alpha R, \tag{3}$$

where R is the propagation distance, α is the attenuation constant and β is the phase shifting constant. According to [36], α and β can be given as follows

$$\alpha = 2\pi f_c \sqrt{\frac{\mu\epsilon'}{2}\left[\sqrt{1 + \left(\frac{\epsilon''}{\epsilon'}\right)^2} - 1\right]}, \tag{4}$$

$$\beta = 2\pi f_c \sqrt{\frac{\mu\epsilon'}{2}\left[\sqrt{1 + \left(\frac{\epsilon''}{\epsilon'}\right)^2} + 1\right]}, \tag{5}$$

where f_c is the central frequency, μ is the magnetic permeability, ϵ' and ϵ'' are the real and imaginary parts of the relative dielectric constant of the soil-water mixture, which can be calculated as

$$\epsilon' = 1.15\left[1 + \frac{\rho_b}{\rho_s}(\epsilon_s)^{\alpha'} + (m_v)^{\beta'}\left(\epsilon'_{f_w}\right)^{\alpha'} - m_v\right]^{1/\alpha'} - 0.68, \tag{6}$$

$$\epsilon'' = \left[(m_v)^{\beta''}\left(\epsilon''_{f_w}\right)^{\alpha'}\right]^{1/\alpha'}. \tag{7}$$

Therein, ρ_b is the bulk density, $\rho_s = 2.66\ \mathrm{g/cm^3}$ is the specific density of solid soil particles and m_v is the volumetric water content (VWC) of the soil. $\alpha' = 0.65$, $\beta' = 1.2748 - 0.519\ S - 0.152\ C$, and $\beta'' = 1.33797 - 0.603\ S - 0.166\ C$ are empirically determined constants, where S and C stand for the mass fractions of sand and clay, respectively. ϵ'_{f_w} and ϵ''_{f_w} are the real and imaginary parts of the relative dielectric constant of water. The value of $\epsilon_s = (1.01 + 0.44\rho_s)^2 - 0.062$ is calculated for a given ρ_s [37].

Once the soil characteristics and the transmitting power are known, the relationship between propagation distance and received signal strength is determined. According to the relationship between them, if P_r is known, R can be obtained and used for localization. Vice versa, if R is known, P_r can also be derived and used for theoretical BER calculation.

For LoRa communication, it is not sufficient to consider only large-scale propagation effects but also the variation due to small-scale propagation effects. It is worth noting that objects such as roots, stones, and clay particles in the soil reflect and refract EM waves just like obstacles in the air. Hence, the randomness of the underground environment still follows the Rayleigh probability distribution [38].

Consequently, we consider a frequency-flat and slow Rayleigh fading channel between each transmitter and receiver. The complex channel coefficient h_i between the transmitter

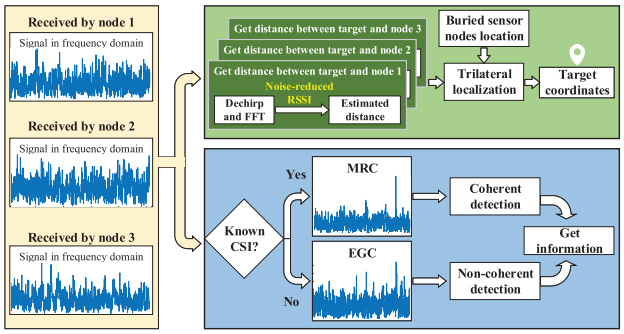

Fig. 3. Flowchart of the joint communication and localization processing using the received signals from each node.

and the i-th receiver has a Rayleigh-distributed amplitude a_i and uniform phase θ_i, denoted as below

$$h_i = a_i e^{j\theta_i}, \tag{8}$$

Based on such a channel model, the received signal $r_i(nT)$ mixed with noise can be expressed as

$$r_i(nT) = h_i s_m(nT) + n_i, \tag{9}$$

where n_i is the complex additive white Gaussian noise (AWGN). Since the preamble is a known sequence of upchirps, it can be used to perform channel estimation for h_i and thus provide assistance for later demodulation operations.

IV. Joint Communication and Localization Operations in LoRaAid

After propagation through underground channel, the received signals $r_i(nT)$ from multiple nodes are further combined so as to realize signal demodulation and target localization simultaneously. Two different LoRa demodulation algorithms namely coherent demodulation and non-coherent demodulation, can be used according to the limitations of hardware equipment and communication overhead as well as the requirement of precision in different scenarios. In addition, the target position can be obtained by the trilateration localization algorithm based on the noise-reduced RSSI. The specific scheme is shown in Fig. 3.

A. Data Transmission Based on Multiple Nodes

Depending on whether the channel-state-information (CSI) is obtained, MRC with coherent demodulation or EGC with non-coherent demodulation can be used for M received signals, respectively. The former can achieve full diversity order, but it requires accurate channel estimation, resulting in additional training overhead and high complexity. The latter has limited SNR improvement but is easy to implement.

1) LoRa Coherent Demodulation With MRC: In coherent demodulation, perfect knowledge of CSI is assumed to be known and used to perform the maximal ratio combining for M received signals. Specifically, the MRC diversity combiner generates the sum of $r_i(nT)$ multiplied by the complex conjugate of channel coefficients as follows

$$y(nT) = \sum_{i=1}^{M} h_i^* r_i(nT) = \sum_{i=1}^{M} h_i^* (h_i s_m(nT) + n_i)$$
$$= \left(\sum_{i=1}^{M} a_i^2 \right) s_m(nT) + \bar{n}, \tag{10}$$

where $\bar{n}$ denotes the noise after the multiplication operation. After obtaining the coherent combined signal, the standard LoRa coherent demodulation and decoding operations are performed to extract the payload data. The output of the correlator in the LoRa demodulator is written as

$$\Omega_k = \sum_{n=0}^{2^{SF}-1} y(nT) \cdot s_k^*(nT)$$
$$= \begin{cases} \left(\sum_{i=1}^{M} a_i^2 \right) \sqrt{E_s} + \phi_k, & k = m \\ \phi_k, & k \neq m \end{cases} \tag{11}$$

where $s_k^*(nT)$ is the complex conjugate of the kth basis function, and ϕ_k is the complex Gaussian noise process corresponding to $\bar{n}$. Hence, the transmitted symbol m can be estimated as

$$\hat{m} = \arg \max_{k=0,\ldots,2^{\mathrm{SF}}-1} \left(|\Omega_k| \right), \tag{12}$$

where $|\cdot|$ denotes absolute operation. The data center can obtain information by performing the above process on received signals from multiple nodes. In order to prove the improvement of communication performance by spatial diversity and provide theoretical guidance for practical engineering, we analyze the theoretical BER of underground LoRa modulation with diversity as follows.

Theoretical BER Analysis of Coherent Demodulation Scheme: In a uniform scattering environment with omnidirectional transmit and receive antennas, the minimum antenna separation required for independent fading on each antenna is approximately one half-wavelength [40]. In our scenario, since the distance between different LoRa nodes is more than ten times the wavelength, it can be assumed that each receiving branch is independent of each other. Solving the theoretical BER problem for diversity reception of underground LoRa signals can be viewed as computing the average BER of LoRa under M-fold diversity, assuming that each branch is independent and identically distributed Rayleigh fading. Moment generating function (MGF) is an effective tool that can greatly simplify the performance analysis of the average symbol error probability over fading channels both with and without diversity. Expressing the average error probability using MGF of γ instead of its distribution generally eliminates the difficulty of integration. In particular, when the diversity fading paths are independent of each other, the average error probability of the γ-based MGF is usually in closed form and can be easily computed numerically. Therefore, we use the MGF technique to carry out the theoretical BER derivation for underground LoRa signal reception with diversity.

The derivation of exact closed-form expressions of LoRa BER performance in AWGN fading channel can be given as

follows [39]:

$$P_{AWGN} = \frac{2^{\mathrm{SF}-1}}{2^{\mathrm{SF}}-1} \sum_{q=1}^{2^{\mathrm{SF}}-1} \frac{(-1)^{q+1}}{q+1} \binom{2^{\mathrm{SF}}-1}{q} \cdot e^{-\frac{q}{q+1}\gamma \cdot 2^{\mathrm{SF}}}. \tag{13}$$

where γ represents SNR which can be calculated by the relationship between LoRa SNR and the received signal strength:

$$\gamma = P_r + 174 - 10\log(\mathrm{BW}) - \mathrm{NF}. \tag{14}$$

Therein, the receiver architecture noise figure NF is measured to be 6 dB [16]. Assuming $c_1 = \frac{(-1)^{q+1}}{q+1}\binom{2^{\mathrm{SF}}-1}{q}$ and $c_2 = \frac{q}{q+1} \cdot 2^{\mathrm{SF}}$, Eq. (13) can be rewritten as an exponential function of γ:

$$P_{AWGN} = \frac{2^{\mathrm{SF}-1}}{2^{\mathrm{SF}}-1} \sum_{q=1}^{2^{\mathrm{SF}}-1} c_1 e^{-c_2\gamma}. \tag{15}$$

By using numerical integration, the average probability of LoRa communication with diversity is calculated as

$$P_{UG} = \int_0^{\infty} \frac{2^{SF-1}}{2^{SF}-1} \sum_{q=1}^{2^{SF}-1} c_1 e^{-c_2\gamma} p_{\gamma_\Sigma}(\gamma) d\gamma, \tag{16}$$

where the combiner SNR γ_Σ represents the sum of γ_i. We assume that the branch SNRs are independent so that their joint distribution becomes a product of the individual distributions: $p_{\gamma_1,\ldots,\gamma_M}(\gamma_1,\ldots,\gamma_M) = p_{\gamma_1}(\gamma_1)\ldots p_{\gamma_M}(\gamma_M)$. Using this factorization and substituting $\gamma = \gamma_1 + \cdots + \gamma_M$ in Eq. (16) yields

$$P_{UG} = \underbrace{\int_0^{\infty} \cdots \int_0^{\infty}}_{M\text{-fold}} \frac{2^{SF-1}}{2^{SF}-1} \sum_{q=1}^{2^{SF}-1} c_1 e^{-c_2(\gamma_1+\cdots+\gamma_M)} p_{\gamma_1}(\gamma_1)\ldots p_{\gamma_M}(\gamma_M)\, d\gamma_1 \ldots d\gamma_M. \tag{17}$$

To simplify the above equation, we use the product forms $e^{-c_2(\gamma_1+\cdots+\gamma_M)} = \prod_{i=1}^{M} e^{-c_2\gamma_i}$ and $p_{\gamma_1}(\gamma_1)\ldots p_{\gamma_M}(\gamma_M) = \prod_{i=1}^{M} p_{\gamma_i}(\gamma_i)$. Moreover, we switch the order of integration and multiplication to obtain the desired final form:

$$P_{UG} = \frac{2^{SF-1}}{2^{SF}-1} \sum_{q=1}^{2^{SF}-1} c_1 \prod_{i=1}^{M} \int_0^{\infty} e^{-c_2\gamma_i} p_{\gamma_i}(\gamma_i)\, d\gamma_i, \tag{18}$$

Since the error probability of LoRa modulation in AWGN can be expressed as an exponential function of γ, the MGF method can be used to calculate the average error probability of fading channels with diversity. For a nonnegative random variable γ with distribution $p_\gamma(\gamma), \gamma \geq 0$, MGF is defined as

$$\mathcal{M}_\gamma(s) = \int_0^{\infty} p_\gamma(\gamma) e^{s\gamma} d\gamma. \tag{19}$$

Due to the independence of underground receiving branches, the average probability is just the product of MGFs associated with the SNR on each branch [40]. By substituting the expression of MGF, Eq. (18) can be rewritten as

$$P_{UG} = \frac{2^{\mathrm{SF}-1}}{2^{\mathrm{SF}}-1} \sum_{q=1}^{2^{\mathrm{SF}}-1} c_1 \prod_{i=1}^{M} \mathcal{M}_{\gamma_i}(-c_2), \tag{20}$$

where $\mathcal{M}_{\gamma_i}(s)$ is the MGF of fading distribution for the i-th diversity branch. Since the underground channel satisfies Rayleigh distribution, we use the MGF for Rayleigh distribution as follows

$$\mathcal{M}_{\gamma_i}(s) = (1 - s\bar{\gamma}_i)^{-1}. \tag{21}$$

Therein, $\bar{\gamma}_i$ is the average received SNR of the ith branch. Substituting c_1, c_2 and Eq. (21) back into Eq. (20), we can obtain the theoretical BER for underground LoRa reception with spatial diversity as below

$$P_{UG} = \frac{2^{\mathrm{SF}-1}}{2^{\mathrm{SF}}-1} \sum_{q=1}^{2^{\mathrm{SF}}-1} (-1)^{q+1} \binom{2^{\mathrm{SF}}-1}{q} \cdot \frac{(q+1)^{M-1}}{\prod_{i=1}^{M}(q+1+q2^{\mathrm{SF}}\bar{\gamma}_i)}. \tag{22}$$

Once the soil characteristics and propagation distance are determined, the received signal strength P_r can be calculated using Eqs. (2)-(3), and the theoretical BER is available according to Eqs. (14)-(22).

2) LoRa Non-Coherent Demodulation With EGC: Coherent demodulation with MRC requires knowledge of the time-varying SNR on each branch, which can be difficult to measure. Another equivalent low complexity method using non-coherent demodulation with EGC can also be utilized.

In order to compensate for the phase difference between the signals from different nodes for combination, we can multiply $r_1(nT)$ with the conjugate of $r_2(nT)$ denoted as $r_2^*(nT)$, which is represented as follows:

$$\begin{aligned} &r_1(nT) \cdot r_2^*(nT) \\ &\quad = (h_1 s_m(nT) + n_1) \cdot (h_2^* s_m(nT)^* + n_2^*) \\ &\quad = \sqrt{E_s} h_1 h_2^* + \tilde{n}, \\ &\quad = \sqrt{E_s} a_1 a_2 e^{j(\theta_1 - \theta_2)} + \tilde{n} \end{aligned} \tag{23}$$

where $\tilde{n}$ denotes noises after conjugate multiplication and the value of $\theta_1 - \theta_2$ corresponds to the phase difference between channels h_1 and h_2. By extracting the phase of $r_1(nT) \cdot r_2^*(nT)$, the channel phase difference can be obtained and compensated for signal combination. Let $\Delta\phi_{ij}$ denote the phase difference between signals of i-th and jth nodes. The EGC of M nodes is represented below.

$$z(nT) = r_1(nT) + \sum_{i=2}^{M} r_i(nT) \cdot e^{-j\Delta\phi_{i1}}, \tag{24}$$

where $e^{-j\Delta\phi_{i1}}$ rotates the phase of $r_i(nT)$ to align with the signals of the first node.

After combining the weak signals of multiple nodes, the obtained SNR-enhanced signal $z(nT)$ is sent into LoRa non-coherent demodulation process. Specifically, the received signal undergoes dechirping first and then energy detection using fast Fourier transform (FFT). The dechirping signal is an inverted chirp (downchirp) with no frequency offset represented as follows

$$s^\star(nT) = \sqrt{\frac{1}{2^{\mathrm{SF}}}} e^{-j2\pi \frac{n^2}{2^{\mathrm{SF}+1}}}. \tag{25}$$

The combined signal $z(nT)$ is mixed with the above-mentioned $s^{\star}(nT)$ and the resulting signal is given as

$$w(nT) = z(nT)s^{\star}(nT). \tag{26}$$

By using the FFT operation to detect the energy, the demodulation of the signal can be realized. Accordingly, the modulated symbol denoted as $\hat{m} \in \{0, 1, \ldots, 2^{\mathrm{SF}} - 1\}$ is retrieved as follows,

$$\hat{m} = \left\lfloor \underset{f}{\operatorname{argmax}}[W(f)] \right\rceil, \tag{27}$$

where $W(f)$ is the FFT transform of $w(nT)$. $\lfloor . \rceil$ is the rounding function representing the hard-decision process.

Both coherent and non-coherent demodulation schemes can be used to obtain signals with greatly enhanced SNR. Depending on the conditions of the environment and equipment, one of them can be selected to get the information. Since the theoretical BER for non-coherent demodulation does not have a closed-form expression, it is not described here. The performance of non-coherent demodulation is usually about 2 dB worse than that of coherent demodulation in Rayleigh fading channels [41].

B. Noise-Reduced Underground Localization Algorithm

The localization algorithm can be divided into a range-based localization algorithm and a range-free localization algorithm. In the underground rescue environment, the high density of beacon nodes cannot be guaranteed, so it is more appropriate to use a range-based localization algorithm in this case. At present, common ranging techniques mainly include RSSI, time of arrival (TOA), time difference of arrival (TDOA), angle of arrival (AOA), and so on. Although the last three methods have high accuracy in theory, they are difficult to be widely applied in underground environments due to their complex hardware and high cost. Therefore, LoRaAid uses RSSI for underground trilateral localization.

It is obvious that obtaining R_i according to the RSSI of different receiving nodes is the cornerstone of localization. It should be noted that the underground environment has large attenuation, and the RSSI obtained directly may be significantly affected by noise. An average noise level of -103 dBm is measured in an underground environment [36]. Although the noise may vary with soil properties, this value is representative. According to [36], when the transmission distance is 5 m and transmit power is set to 20 dBm, the RSSI is lower than -110 dBm and drowned by noise. Therefore, it is crucial to reduce the noise of the received signal and obtain accurate RSSI. To this end, the main points of our proposed algorithm include the following two steps:

- **Obtain accurate estimated distance:** Accurate estimated distance based on noise-reduced RSSI is the cornerstone of precise localization.
- **Calculate target coordinates:** The estimated location of the transmitter is obtained by the intersection of the circles corresponding to different receiving nodes.

The following content elaborates on the above components, providing the technical details.

1) Obtain Accurate Estimated Distance: By combining Eqs. (2)-(3), we get the relationship between the received signal power and distance as

$$\underbrace{P_r^i - P_t - G_t - G_r^i - 6.4 - 20\log\beta}_{g(R_i)} = 20\log R_i + 8.69\alpha R_i, \tag{28}$$

where P_r^i is the received signal power of the i-th node, P_t is the transmit power, G_t is the gain of the transmitting antenna, and G_r^i is the gain of the i-th receiving antenna.

Since $g(R_i)$ is a strictly monotonically increasing function, its inverse function $f(g(R_i))$ must exist. Therefore, the value of R_i is jointly determined by the above factors as

$$R_i = f(P_r^i, P_t, G_t, G_r^i, \alpha, \beta). \tag{29}$$

Given that $P_t, G_t, G_r^i, \alpha, \beta$ are known, the focus is on the solution of P_r^i. Intuitively, P_r^i can be obtained from the amplitude of signal $r_i(nT)$. However, the SNR of the signal in an underground environment is extremely low, so we need to perform a noise reduction process. Since the underground noise is approximately uniformly distributed in the frequency domain, we transform the received time domain signal to the frequency domain to obtain the noise-reduced RSSI. Specifically, the received signal undergoes dechirping first and then energy detection using FFT. The received signal $r_i(nT)$ is mixed with the above-mentioned $s^{\star}(nT)$ and the resulting signal is given as follows

$$\begin{aligned} y_i(nT) &= r_i(nT)s^{\star}(nT) \\ &= h_i s(nT)s^{\star}(nT) + \hat{n}_i. \end{aligned} \tag{30}$$

While the noise is multiplied with the dechirping signal, it still maintains its distribution and is represented here as $\hat{n}_i$. By using the FFT operation to detect the energy of the signal and extract the peak value of power spectral density (PSD), the RSSI of the time domain signal can be obtained. Accordingly, the noise-reduced RSSI denoted as $\tilde{P}_r^i$ and the modulated symbol denoted as $\hat{m} \in \{0, 1, \ldots, 2^{SF} - 1\}$ are retrieved as below

$$\tilde{P}_r^i = \frac{\max[Y_i(f)]}{N}, \tag{31}$$

where $Y_i(f)$ is the FFT transform of $y_i(nT)$ and N represents the size of FFT. With this method, accurate RSSI can be acquired even when the signal is submerged in noise.

Consequently, once the received signal $r_i(nT)$ is obtained through node i, it is processed to obtain the accurate $\tilde{P}_r^i$. Therefore, Eq. (29) can be rewritten as

$$R_i = f(\tilde{P}_r^i, P_t, G_t, G_r^i, \alpha, \beta). \tag{32}$$

Although R_i has no explicit expression, it is a monotonic function with a unique solution, so we can solve it in an ergodic way.

2) Calculate Target Coordinates: Once the estimated distance R_i is obtained, the target coordinates can be solved according to the following relationship

$$R_i\,(x, y) = \sqrt{(x_i - x)^2 + (y_i - y)^2}. \tag{33}$$

Algorithm 1 Noise-Reduced Localization Algorithm

Input: $(x_i, y_i), (x_0, y_0), r_i(t), s^{\star}(t), P_t, G_t, G_r^i, \mu, \epsilon', \epsilon'', f_c, \gamma$;
Output: $(\hat{x}, \hat{y})$.
for $i = 1, 2, 3$ **do**
  Mix the received signal $r_i(t)$ with downchirp signal $s^{\star}(t)$ to get $y_i(t)$.
  Perform FFT operation on $y_i(t)$ and extract the peak value of PSD. $\tilde{P}_r^i$ is thus obtained.
  Calculate propagation distance R_i using the known $\tilde{P}_r^i, P_t, G_t, G_r^i, \alpha$ and β in a ergodic manner.
end
while $||\theta|| > \Gamma$ **do**
  Calculate ΔR and A by substituting the known $(x_i, y_i), (x_0, y_0)$ and R_i into Eq. (37).
  Attain θ by substituting ΔR and A into Eq. (38).
  Update (x_0, y_0) with the calculated θ.
end
return (x_0, y_0) from the last loop, denoted as $(\hat{x}, \hat{y})$.

As Eq. (33) is non-linear, we apply the Taylor series to linearize it [42]. Specifically, we can expand it at the point (x_0, y_0) and omit the second and higher order terms, denoted as follows

$$R_i(x, y) = R_i(x_0, y_0) + \frac{\partial R_i}{\partial x}\Delta x + \frac{\partial R_i}{\partial y}\Delta y, \tag{34}$$

where $\Delta x = x - x_0, \Delta y = y - y_0$. Assuming that $\Delta R_i = R_i(x, y) - R_i(x_0, y_0)$, we have

$$\Delta R_i = \frac{\partial R_i}{\partial x}\Delta x + \frac{\partial R_i}{\partial y}\Delta y. \tag{35}$$

Therefore, according to Eq. (35), we rewrite data from three nodes into a vector form as below.

$$\begin{pmatrix} \Delta R_1 \\ \Delta R_2 \\ \Delta R_3 \end{pmatrix} = \begin{pmatrix} \frac{\partial R_1}{\partial x} & \frac{\partial R_1}{\partial y} \\ \frac{\partial R_2}{\partial x} & \frac{\partial R_2}{\partial y} \\ \frac{\partial R_3}{\partial x} & \frac{\partial R_3}{\partial y} \end{pmatrix} \begin{pmatrix} \Delta x \\ \Delta y \end{pmatrix}. \tag{36}$$

The partial derivative calculation of Eq. (36) is shown as Eq. (37), shown at the bottom of the next page. By solving it, we can obtain a one-time estimation as

$$\theta = \left(A^T A\right)^{-1} A^T \Delta R. \tag{38}$$

Based on this, we replace the initial guess (x_0, y_0) with a new point $(x_0 + \Delta x, y_0 + \Delta y)$ in Eq. (37) to start another round of least square (LS) estimation until the solution converges below a threshold Γ. In our experiments, we set $\Gamma = 0.05$m. In other words, when $\sqrt{(\Delta x)^2 + (\Delta y)^2} < \Gamma = 0.05$m is satisfied, the iteration is stopped. A summary of the localization algorithm is given in Algorithm 1.

C. Energy Consumption Calculations of LoRaAid

LoRa is well known for its low-power performance and can run for years on batteries. In order to investigate the proposed scheme from the perspective of energy consumption and battery life, we give a detailed energy calculation procedure and compare the LoRaAid system with the conventional LoRa system. It is worth noting that the power consumption of the transmitting process is much higher than that of receiving process, and it is difficult to replace the batteries of wearable LoRa devices when people are trapped, so we only focus on the power consumption of the transmitting node.

Total energy consumption includes consumption in sleep mode and active mode. When only the uplink is considered, it can be simplified to the following equation

$$\begin{aligned} E_{total} &= E_{Tx} + E_{sleep} \\ &= V_{supply} I_{Tx} T_{Tx} + V_{supply} I_{sleep} T_{sleep}. \end{aligned} \tag{39}$$

where E_{sleep} is the energy consumed in sleep mode and E_{Tx} is the energy consumption of transmitting signal. V_{supply} is the supply voltage. I_{sleep} is the sleep current, and T_{sleep} is the sleep time, whose length is related to the duty cycle of the signal. The transmitting current I_{Tx} is closely related to P_t. T_{Tx} represents the time on air of the whole package and is determined by the duration of the symbol and the total number of symbols. When the sampling rate is equal to BW, the duration of each symbol is

$$T_{\text{sym}} = \frac{2^{\text{SF}}}{\text{BW}}. \tag{40}$$

The number of symbols is the sum of the preamble and transmitted packet. The preamble length is calculated as follows:

$$T_{\text{preamble}} = (n + 4.25)\, T_{\text{sym}}\,. \tag{41}$$

The following formula gives the number of payload symbols.

$$n_{\text{payload}} = 8 + \max\left(\left\lceil \frac{(8\text{PL} - 4\text{SF} + 28 + 16\text{CRC} - 20\text{IH})}{4(\text{SF} - 2\text{DE})} \right\rceil \cdot \frac{4}{\text{CR}}, 0\right). \tag{42}$$

With the following dependencies:
- CRC is 1 if the CRC check is enabled and otherwise 0.
- IH=0 when the header is enabled, IH=1 otherwise.
- DE=1 when LowDataRateOptimize=1, DE=0 otherwise.

The payload duration is then the symbol period multiplied by the number of payload symbols

$$T_{\text{payload}} = n_{\text{payload}} \times T_{\text{sym}}\,. \tag{43}$$

The packet duration is the sum of the preamble and payload duration.

$$T_{Tx} = T_{\text{preamble}} + T_{\text{payload}}\,. \tag{44}$$

After configuring the parameters of LoRaPHY, the transmission duration can be derived, and the total energy consumption can be finally determined. In our system, due to the use of spatial diversity for signal reception, it is still possible to achieve correct demodulation even with lower SNR. As shown in Fig. 7(a), in the case of single antenna reception, reliable transmission of 6.3m can be achieved by setting SF=12 at the transmitter, while the same performance can be achieved with SF=7 in the case of multiple antenna diversity reception. The reduction of SF leads to a significant decrease in transmission duration, which results in lower total energy consumption. Taking the SX1262 chip as an example, we give specific calculations below.

TABLE I
SX1262 PARAMETER DETAILS

n	CRC	IH	DE	V_{supply}	I_{Tx}	I_{sleep}
8	0	0	0	3.3 V	102mA	1.2μA

1) Single-Node Reception: By using the LoRa calculation tool and querying the product datasheet, the various parameters needed for the calculation are obtained and listed in Table I.

The device sends a message every 60 s with a length of 10 bytes. So the duration of transmitting signal needs to be divided by the duty cycle, $T_{duty} = 60$, to get the average time per second to transmit the signal, as given in Eq. (45), shown at the bottom of the page. The duration of sleep mode is the time remaining in 1 s and can be calculated as

$$T^S_{sleep} = 1000ms - T^S_{Tx} = 985.53\text{ms}. \tag{46}$$

The energy consumption of the transmitting signal is given by

$$\begin{aligned} E^S_{Tx} &= V_{supply} I_{Tx} T^S_{Tx} \\ &= 3.3\text{V} \times 102\text{mA} \times 14.47\text{ms} \\ &= 4.87\ mJ. \end{aligned} \tag{47}$$

The energy consumed in sleep mode is expressed as

$$\begin{aligned} E^S_{sleep} &= V_{supply} I_{sleep} T^S_{sleep} \\ &= 3.3\text{V} \times 1.2\mu\text{A} \times 985.53\text{ms} \\ &= 0.0039\ mJ. \end{aligned} \tag{48}$$

For a 1000 mA·h Lithium battery with a voltage of 3.3 V, it can operate for

$$T^S_{life} = \frac{3.3\ V \times 1000\ mA \times 3600s}{(E^S_{Tx} + E^S_{sleep})} = 28.2\ days. \tag{49}$$

2) Multi-Node Diversity Reception: Following the above derivation and calculating with SF = 12, we get the duration of transmitting signal in Eq. 50, shown at the bottom of the next page. Other results for duration and energy consumption are written as follows.

$$T^M_{sleep} = 1000ms - T^M_{Tx} = 999.41\text{ms}. \tag{51}$$

$$E^M_{Tx} = V_{supply} I_{Tx} T^M_{Tx} = 0.199\ mJ. \tag{52}$$

$$E^M_{sleep} = V_{supply} I_{sleep} T^M_{sleep} = 0.00396\ mJ. \tag{53}$$

$$T^M_{life} = \frac{3.3\ V \times 1000\ mA \times 3600s}{(E^M_{Tx} + E^M_{sleep})} = 677.47\ days. \tag{54}$$

Obviously, our system can withstand much smaller SF and greatly reduce the message transmission time, thus significantly extending the battery life. In practice, due to the instability of batteries, the actual lifespan is usually only half of the calculated lifespan, but it is still possible to achieve more than one year with our system.

V. EXPERIMENTAL SETUP

Some necessary preliminary experimental settings, such as LoRa platform configuration, experimental site and equipment, and soil characteristics, are described in this section.

A. LoRa Platform Configuration

The LoRa frame used in our experiments consists of four parts: the preamble, header, payload, and cyclic redundancy check (CRC). The preamble does not correspond to any information but is utilized for synchronization purposes. It consists of a series of upchirps, a synchronization word with 2 upchirps, and a Start of Frame Delimiter (SFD) with 2.25 downchirps. The length of the initial unmodulated upchirps sequence is typically configured to $n = 8$ in general applications. The header contains information such as payload length and payload coding rate (CR). It has a CR of 4/8 and exists in explicit mode. The payload is where the message is encoded. It contains node identification information, such as the device address (DevAddr), which allows it to be recognized by the gateway [43]. PL denotes the number of payload bytes (1 to 255), and we set PL=10 in our experiments. Finally, it is optional whether to add CRC after the payload. Fig. 4 illustrates the frame structure described above.

LoRa can be characterized by four physical parameters: P_t, SF, BW, and CR, which further affect link quality, data rate, energy consumption, and resistance to interference and noise. P_t ranges from -4 to 20 dBm depending on the deployment area. SF ranges from 7 to 12, indicating the number of bits that can be encoded in the symbol. Higher SF can

$$\underbrace{\begin{pmatrix} R_1 - \sqrt{(x_0-x_1)^2 + (y_0-y_1)^2} \\ R_2 - \sqrt{(x_0-x_2)^2 + (y_0-y_2)^2} \\ R_3 - \sqrt{(x_0-x_3)^2 + (y_0-y_3)^2} \end{pmatrix}}_{\Delta R} = \underbrace{\begin{pmatrix} \frac{x_0-x_1}{\sqrt{(x_0-x_1)^2+(y_0-y_1)^2}} & \frac{y_0-y_1}{\sqrt{(x_0-x_1)^2+(y_0-y_1)^2}} \\ \frac{x_0-x_2}{\sqrt{(x_0-x_2)^2+(y_0-y_2)^2}} & \frac{y_0-y_2}{\sqrt{(x_0-x_2)^2+(y_0-y_2)^2}} \\ \frac{x_0-x_3}{\sqrt{(x_0-x_3)^2+(y_0-y_3)^2}} & \frac{y_0-y_3}{\sqrt{(x_0-x_3)^2+(y_0-y_3)^2}} \end{pmatrix}}_{A} \underbrace{\begin{pmatrix} \Delta x \\ \Delta y \end{pmatrix}}_{\theta}. \tag{37}$$

$$\begin{aligned} T^S_{Tx} &= \frac{\left(n + 4.25 + 8 + \max\left(\left\lceil \frac{(8PL - 4\text{SF} + 28 + 16CRC - 20IH)}{4(\text{SF} - 2DE)} \right\rceil \cdot \frac{4}{\text{CR}}, 0\right)\right) T_{\text{sym}}}{T_{duty}} \\ &= \frac{\left(8 + 4.25 + 8 + \max\left(\left\lceil \frac{(8\times 10 - 4\times 12 + 28)}{4\times 12} \right\rceil \cdot \frac{4}{4/5}, 0\right)\right) \times \frac{2^{12}}{125000}}{60} \\ &= 14.47\text{ms}. \end{aligned} \tag{45}$$

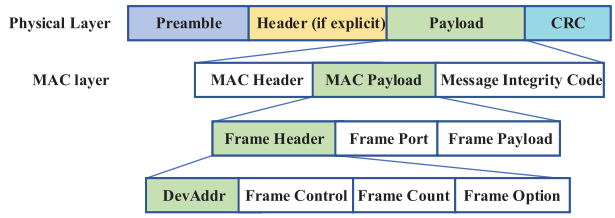

Fig. 4. The physical layer and MAC layer frame structure of LoRa signal.

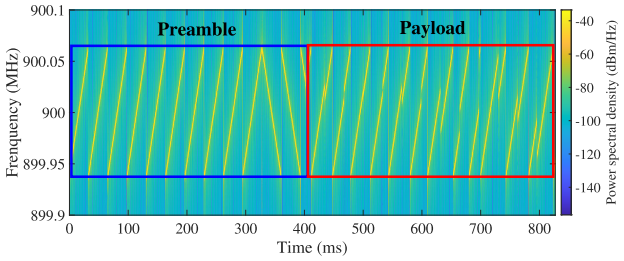

Fig. 5. Spectrogram of LoRa frame with a 10-byte payload.

improve the anti-interference ability of the signal with reduced data rate and increased energy expenditure. BW in LoRa is typically set to 125, 250, and 500 kHz. Higher BW implies a higher data rate and lower packet duration but less sensitivity. CR represents the proportion of the payload in the total data bits. In this paper, we set CR to 4/5. The data rate of LoRa jointly determined by SF, BW, and CR is given as follows:

$$\mathrm{DR} = \mathrm{SF} * \frac{4\mathrm{BW}}{(4+\mathrm{CR})2^{\mathrm{SF}}}. \tag{55}$$

The spectrogram of a LoRa frame is shown in Fig. 5 when the parameters are configured as P_t=20 dBm, SF = 12, BW = 125kHz, CR=4/5, and f_c = 900MHz. According to Eq. (55), the data rate under this parameter configuration can be obtained as DR=5.7 kb/s. To reduce the transmission time, we do not use header and CRC in our experiments.

B. Experimental Site and Equipments

We tested more than 600 different sets of data in a sandy soil field to verify the effectiveness of our proposed LoRaAid system. In order to explore the influence of soil moisture on communication and localization, we carried out experiments on sunny days and after rain. Since the experiments are conducted outdoors, there are certain fluctuations in soil moisture of $5\%\pm1.2\%$, $10\%\pm2.5\%$, and $15\%\pm3.1\%$, respectively. For the convenience of description, it is directly simplified to 5%, 10%, and 15%. The locations of the pre-deployed receivers and random targets are depicted in Fig. 6. In order to explore the limit of LoRa underground communication performance, we set the maximum distance between each receiver and transmitter as 10 m. The burial depth of the antennas is set to be 40 cm. While the communication experiments are carried

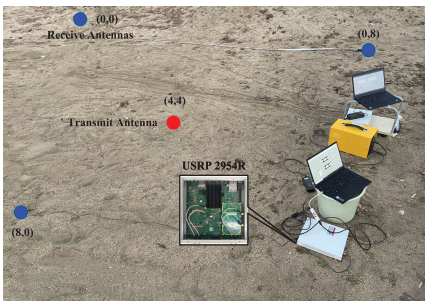

(a) LoRaAid platform (b) Antenna burial depth

Fig. 6. Outdoor experimental field. The blue solid points represent the receiving nodes, and the red solid point represents the transmitting node, which is also the target to be located.

TABLE II
SOIL CHARACTERISTICS PARAMETERS

P_t	G_t	G_r	f_c	S	C	ρ_b	μ	ϵ_0
20 dBm	0 dB	0 dB	900 MHz	90%	10%	1.5 $\mathrm{g/cm^3}$	$4\pi \times 10^{-7}$H/m	8.854×10^{-12}F/m

out at various distances, the received signals on each node are also used in the localization algorithm to obtain the target position. We implement our system with two USRP 2954Rs, and each of them is connected to a PC with 16 GB memory and an Intel i7 dual-core processor. The USRPs work at central frequency f_c = 900 MHz and adopt omnidirectional VERT 900 antennas.

The soil-related parameters, such as the soil texture, bulk density, magnetic permeability, and electrical conductivity, are listed in Table II. Other parameters that affect RSSI, such as antenna gain and transmit power, are also shown in it.

VI. Experimental Results

We mainly evaluate the system in three aspects: communication reliability, localization accuracy, and energy consumption. In order to evaluate the communication performance of the system, the bit error rate (BER) of the system under different soil moisture and parameter configurations is simulated according to the theoretical derivation in Section IV, and then the actual experimental results are compared with the theoretical results. The position error is characterized by Euclidean distance between the estimated coordinates $(\hat{x}, \hat{y})$ and actual coordinates (x, y) expressed as $\sqrt{(\hat{x}-x)^2+(\hat{y}-y)^2}$. The localization performance of the LoRaAid system is evaluated experimentally in terms of both soil moisture and noise reduction algorithm, respectively.

A. Communication Performance of LoRaAid

The theoretical BER results of underground LoRa signal transmission derived from Section IV are shown in

$$T_{Tx}^{M} = \frac{\left(8+4.25+8+\max\left(\left\lceil\frac{(8\times10-4\times7+28)}{4\times7}\right\rceil\cdot\frac{4}{4/5},0\right)\right)\times\frac{2^7}{125000}}{60} = 0.59\mathrm{ms}. \tag{50}$$

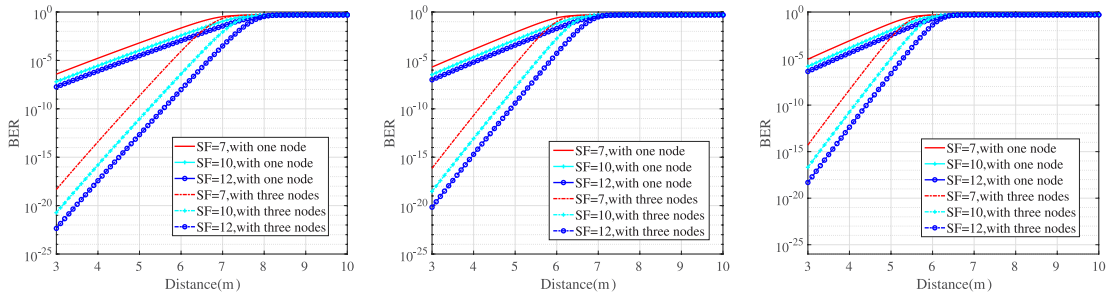

(a) m_v=5%. (b) m_v=10%. (c) m_v=15%.

Fig. 7. Theoretical BER of underground communication performance under different soil moisture with BW=125kHz. The number of nodes for diversity reception is set to 3, and SF is taken as 7, 10, and 12 at each soil moisture level.

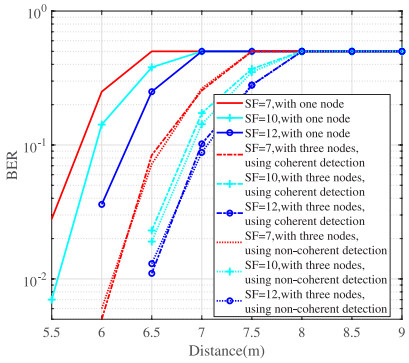

Fig. 8. Underground communication performance with different numbers of nodes at the soil moisture of 5%.

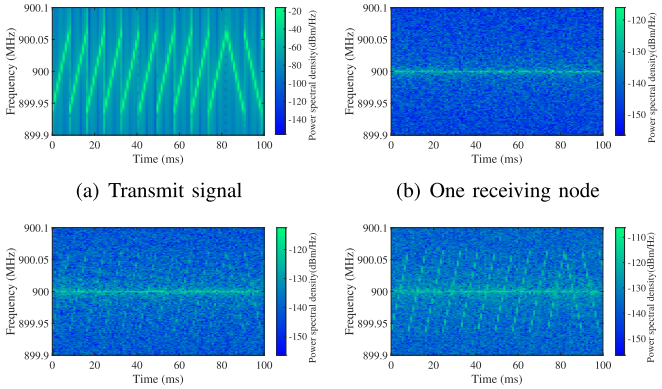

(a) Transmit signal (b) One receiving node

(c) Three receiving nodes (d) Eight receiving nodes

Fig. 9. Spectrogram of combined signals with different numbers of nodes, where SF=10 and BW=125kHz.

Fig. 7. In fact, Matlab suffers from precision problems and returns infinity for the calculation of binomial coefficients $\binom{2^{\mathrm{SF}}-1}{q}$ when SF is greater than 5, so the calculation can only be implemented by using the gmpy2 package in Python.[1] The simulation results of the theoretical bit error rate show that the use of spatial diversity can significantly improve the transmission reliability of underground LoRa signals. This is because a more favorable SNR distribution can be achieved when multiple independently fading received signals are combined. And with the decrease of SF and the increase of soil moisture, the achievable distance gradually decreases.

Through the experimental results presented in Fig. 8, it can be seen that the correct combination of multiple received signals can significantly improve LoRa modulation performance, thus expanding the coverage. Both signal combination methods can extend the maximum transmission distance by about 1m. The actual experimental results are basically equivalent to the theoretical values of the coherent demodulation scheme. Theoretically, the performance of the scheme using MRC and coherent demodulation will be superior. However, since the channel estimation is not accurate enough, it is actually similar to that of EGC and non-coherent demodulation.

Fig. 9 shows the spectrogram of the signal with diversity when non-coherent demodulation is used. The signal received by a single node cannot be demodulated because the signal is too weak. LoRa chirp starts to appear when the signals received by three nodes are combined and becomes clearer when the number of nodes increases to eight. This is because as the number of nodes increases, the SNR of the combined signal becomes larger, and the amplitude of FFT increases, making it easier to achieve the correct demodulation.

BER results of actual experiments for various LoRa physical parameters are shown in Fig. 10. The variables are SF and BW, and other conditions are kept the same. For example, soil moisture is 5%, and the coherent demodulation scheme is used. A common feature observed in all cases is that BER increases with smaller SF and wider BW. Indeed, wide BW implies an increase in the data rate. However, it also leads to a degradation in receiving sensitivity and hence a significant rise in BER. Second, when the SF increases from 7 to 12, the data rate is reduced in exchange for an increase in link quality, which extends the propagation distance but requires a larger packet symbol size and higher energy consumption. Therefore, a moderate SF should be used for the tradeoff between link performance and energy consumption. According to the link performance under different parameters, it can be seen that the communication is very reliable by using the combination of multiple nodes. For example, the BER of the UG2UG channel with the configuration of (7,500,4/5) attains 0.5 as the distance exceeds 7.5 m, which means a complete inability to transmit information. This represents the worst case among all physical parameter configurations, but the reliable transmission range is quite sufficient for our scenario.

[1]The code for theoretical BER calculation is available on the following website: https://github.com/HuaijinZhang/Underground-LoRaAid.

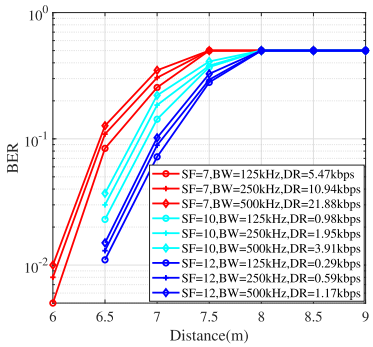

Fig. 10. Underground communication performance with different physical layer parameter configurations at the soil moisture of 5%.

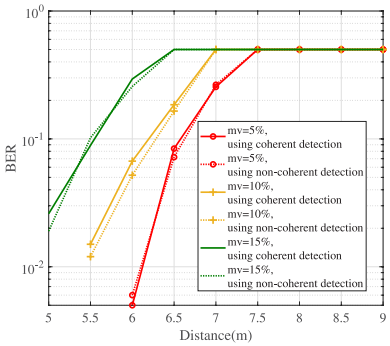

Fig. 11. Underground communication performance under different soil moisture with SF=7 and BW=125kHz.

The variation of path loss with soil moisture leads to a change in communication coverage. Fig. 11 indicates that the communication reachable distance gradually decreases from 7.5m to 6.5m with the increase of soil moisture from 5% to 15%. This is due to the fact that larger m_v leads to higher relative permittivity of the soil, resulting in a change in wavelength and thus affecting the signal attenuation. The SNR gradually approaches the threshold after the attenuation increases, making it harder to demodulate the signal correctly.

B. Localization Accuracy of LoRaAid

In order to explore the influence of noise-reduced localization algorithm on localization accuracy, m_v is set to 5% and 15% to verify the effectiveness of using $\tilde{P}_r^i$ instead of P_r^i. Fig. 12(a) shows the cumulative distribution function (CDF) of position error with and without noise reduction, and Fig. 12(b) plots the localization results, including both mean accuracy and standard deviation. It can be seen that with the increase of soil moisture, the advantages of noise-reduced localization algorithm gradually become prominent. For example, at the CDF of 90%, the gap between using and not using the noise-reduced algorithm is 0.1 m for $m_v = 5\%$ and 0.3 m for $m_v = 15\%$. According to Fig. 12, after using the noise-reduced algorithm, the average localization accuracy is improved by 8% when $m_v = 5\%$, and 18% when $m_v = 15\%$. It is due to the fact that the increase in soil moisture leads to a smaller discrepancy between noise and signal strength, which makes the advantage of the noise-reduced algorithm more apparent.

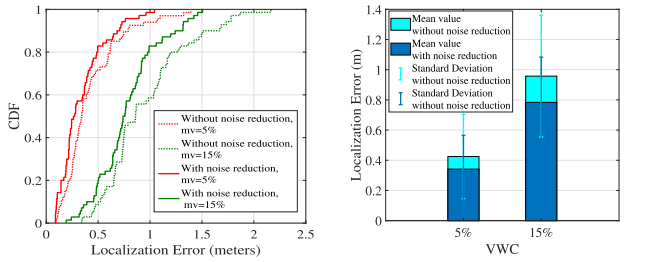

(a) CDF of the position error (b) Mean and standard deviation of position error

Fig. 12. The impact of noise-reduced localization algorithm on localization accuracy.

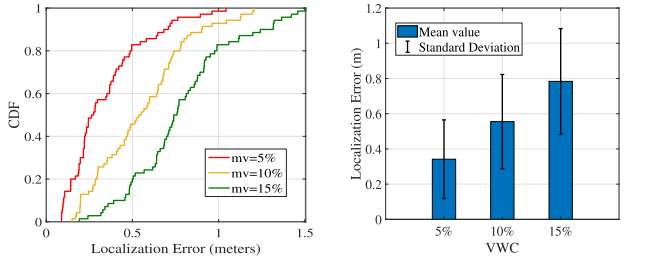

(a) CDF of the position error (b) Mean and standard deviation of position error

Fig. 13. Impact of the soil moisture on localization accuracy.

To illustrate the soil moisture effects, different VWC levels are considered between 5% and 15%. As shown in Fig. 13(a), when $m_v = 10\%$, the median and 90% position error are 0.57m and 0.91m, respectively. While at a VWC level of 15%, both of them become higher, reaching 0.78m and 1.25m, respectively. It can be seen from Fig. 13(b) that the mean position error is initially around 0.34 m and increases to 0.79 m in the case of $m_v = 15\%$. A 10% increase in VWC reduces the localization accuracy by at least 0.45 m. This is due to the fact that the larger m_v is, the more difficult it is to accurately obtain RSSI, resulting in greater positioning error.

VII. Conclusion

This paper presented the design, implementation, and performance evaluation of a joint communication and localization system called LoRaAid for underground emergency rescue. LoRaAid combined signals from multiple nodes to improve the reliability of transmission and localize the target node simultaneously. To achieve diversity reception of signals, two different schemes have been proposed, namely coherent demodulation with MRC and non-coherent demodulation with EGC. Meanwhile, LoRaAid used the RSSI of different receivers to calculate the distance and perform trilateral localization accordingly. In particular, considering that high signal attenuation can seriously affect the accuracy of RSSI, we proposed a noise reduction algorithm to reduce the localization error. The effects of LoRa parameters and soil moisture on communication reliability and localization accuracy have also been analyzed through simulations and practical measurements. The results proved that our system could achieve decimeter-level positioning accuracy even at communication distances of up to 7 m. In addition, energy consumption has been greatly reduced

with longer battery life. We believe that the outstanding advantages of LoRaAid will promote the development of underground rescue in the future.

REFERENCES

[1] Z. Li, Z. Sun, T. Singh, and E. Oware, "Large range soil moisture sensing for inhomogeneous environments using magnetic induction networks," in *Proc. IEEE Global Commun. Conf. (GLOBECOM)*, Dec. 2019, pp. 1–6.

[2] H. Guo and A. A. Ofori, "The Internet of Things in extreme environments using low-power long-range near field communication," *IEEE Internet Things Mag.*, vol. 4, no. 1, pp. 34–38, Mar. 2021.

[3] G. Liu, "A Q-learning-based distributed routing protocol for frequency-switchable magnetic induction-based wireless underground sensor networks," *Future Gener. Comput. Syst.*, vol. 139, pp. 253–266, Feb. 2023.

[4] X. Tan, Z. Sun, and I. F. Akyildiz, "Wireless underground sensor networks: MI-based communication systems for underground applications," *IEEE Antennas Propag. Mag.*, vol. 57, no. 4, pp. 74–87, Aug. 2015.

[5] Z. Sun, I. F. Akyildiz, and G. P. Hancke, "Dynamic connectivity in wireless underground sensor networks," *IEEE Trans. Wireless Commun.*, vol. 10, no. 12, pp. 4334–4344, Dec. 2011.

[6] N. Saeed, M.-S. Alouini, and T. Y. Al-Naffouri, "Toward the Internet of Underground Things: A systematic survey," *IEEE Commun. Surveys Tuts.*, vol. 21, no. 4, pp. 3443–3466, 4th Quart., 2019.

[7] G. Liu, "Data collection in MI-assisted wireless powered underground sensor networks: Directions, recent advances, and challenges," *IEEE Commun. Mag.*, vol. 59, no. 4, pp. 132–138, Apr. 2021.

[8] Z. Sun and I. F. Akyildiz, "Optimal deployment for magnetic induction-based wireless networks in challenged environments," *IEEE Trans. Wireless Commun.*, vol. 12, no. 3, pp. 996–1005, Mar. 2013.

[9] A. Salam, M. C. Vuran, and S. Irmak, "A statistical impulse response model based on empirical characterization of wireless underground channels," *IEEE Trans. Wireless Commun.*, vol. 19, no. 9, pp. 5966–5981, Sep. 2020.

[10] H. Guo, Z. Sun, and C. Zhou, "Practical design and implementation of metamaterial-enhanced magnetic induction communication," *IEEE Access*, vol. 5, pp. 17213–17229, 2017.

[11] G. Liu, Z. Wang, and T. Jiang, "QoS-aware throughput maximization in wireless powered underground sensor networks," *IEEE Trans. Commun.*, vol. 64, no. 11, pp. 4776–4789, Nov. 2016.

[12] G. Liu, Z. Sun, and T. Jiang, "Joint time and energy allocation for QoS-aware throughput maximization in MIMO-based wireless powered underground sensor networks," *IEEE Trans. Commun.*, vol. 67, no. 2, pp. 1400–1412, Feb. 2019.

[13] X.-F. Wan, Y. Yang, J. Cui, and M. S. Sardar, "LoRa propagation testing in soil for wireless underground sensor networks," in *Proc. 6th Asia–Pacific Conf. Antennas Propag. (APCAP)*, Oct. 2017, pp. 1–3.

[14] B. Zhou, V. S. S. L. Karanam, and M. C. Vuran, "Impacts of soil and antenna characteristics on LoRa in Internet of Underground Things," in *Proc. IEEE Global Commun. Conf. (GLOBECOM)*, Dec. 2021, pp. 1–6.

[15] G. Di Renzone, S. Parrino, G. Peruzzi, A. Pozzebon, and D. Bertoni, "LoRaWAN underground to aboveground data transmission performances for different soil compositions," *IEEE Trans. Instrum. Meas.*, vol. 70, pp. 1–13, 2021.

[16] K. Lin and T. Hao, "Experimental link quality analysis for LoRa-based wireless underground sensor networks," *IEEE Internet Things J.*, vol. 8, no. 8, pp. 6565–6577, Apr. 2021.

[17] K. Lin and T. Hao, "Adaptive selection of transmission configuration for LoRa-based wireless underground sensor networks," in *Proc. IEEE Wireless Commun. Netw. Conf. (WCNC)*, Mar. 2021, pp. 1–6.

[18] K. Lin and T. Hao, "Link quality analysis of wireless sensor networks for underground infrastructure monitoring: A non-backfilled scenario," *IEEE Sensors J.*, vol. 21, no. 5, pp. 7006–7014, Mar. 2021.

[19] N. Hou, X. Xia, and Y. Zheng, "Don't miss weak packets: Boosting LoRa reception with antenna diversities," in *Proc. IEEE INFOCOM Conf. Comput. Commun.*, May 2022, pp. 530–539.

[20] R. K. Sharma and A. K. Gupta, "Continuous wave acoustic method for determination of moisture content in agricultural soil," *Comput. Electron. Agricult.*, vol. 73, no. 2, pp. 105–111, Aug. 2010.

[21] F. Miramirkhani, M. Uysal, O. Narmanlioglu, M. Abdallah, and K. Qaraqe, "Visible light channel modeling for gas pipelines," *IEEE Photon. J.*, vol. 10, no. 2, pp. 1–10, Apr. 2018.

[22] X. Dong and M. C. Vuran, "A channel model for wireless underground sensor networks using lateral waves," in *Proc. IEEE Global Telecommun. Conf.*, Dec. 2011, pp. 1–6.

[23] A. Salam and M. C. Vuran, "Wireless underground channel diversity reception with multiple antennas for Internet of Underground Things," in *Proc. IEEE Int. Conf. Commun. (ICC)*, May 2017, pp. 1–7.

[24] A. F. C. Errington, B. L. F. Daku, and A. F. Prugger, "Initial position estimation using RFID tags: A least-squares approach," *IEEE Trans. Instrum. Meas.*, vol. 59, no. 11, pp. 2863–2869, Nov. 2010.

[25] J. Wang, Y. Guo, L. Guo, B. Zhang, and B. Wu, "Performance test of MPMD matching algorithm for geomagnetic and RFID combined underground positioning," *IEEE Access*, vol. 7, pp. 129789–129801, 2019.

[26] M. D. Bedford and G. A. Kennedy, "Evaluation of ZigBee (IEEE 802.15.4) time-of-flight-based distance measurement for application in emergency underground navigation," *IEEE Trans. Antennas Propag.*, vol. 60, no. 5, pp. 2502–2510, May 2012.

[27] H. Zemmour, G. Baudoin, and A. Diet, "Soil effects on the underground-to-aboveground communication link in ultrawideband wireless underground sensor networks," *IEEE Antennas Wireless Propag. Lett.*, vol. 16, pp. 218–221, 2017.

[28] M. Pang, G. Shen, X. Yang, K. Zhang, P. Chen, and G. Wang, "Achieving reliable underground positioning with visible light," *IEEE Trans. Instrum. Meas.*, vol. 71, pp. 1–15, 2022.

[29] S. Bastiaens, S. K. Goudos, W. Joseph, and D. Plets, "Metaheuristic optimization of LED locations for visible light positioning network planning," *IEEE Trans. Broadcast.*, vol. 67, no. 4, pp. 894–908, Dec. 2021.

[30] B. Meunier et al., "Visible light positioning with lens compensation for non-Lambertian emission," *IEEE Trans. Broadcast.*, vol. 69, no. 1, pp. 289–302, Mar. 2023.

[31] L. Shi, B. Béchadergue, L. Chassagne, and H. Guan, "Joint visible light sensing and communication using m-CAP modulation," *IEEE Trans. Broadcast.*, vol. 69, no. 1, pp. 276–288, Mar. 2023.

[32] S.-C. Lin, A. A. Alshehri, P. Wang, and I. F. Akyildiz, "Magnetic induction-based localization in randomly deployed wireless underground sensor networks," *IEEE Internet Things J.*, vol. 4, no. 5, pp. 1454–1465, Oct. 2017.

[33] N. Saeed, M.-S. Alouini, and T. Y. Al-Naffouri, "3D localization for Internet of Underground Things in oil and gas reservoirs," *IEEE Access*, vol. 7, pp. 121769–121780, 2019.

[34] S. Kisseleff, X. Chen, I. F. Akyildiz, and W. Gerstacker, "Localization of a silent target node in magnetic induction based wireless underground sensor networks," in *Proc. IEEE Int. Conf. Commun. (ICC)*, May 2017, pp. 1–7.

[35] H. Ma, G. Cai, Y. Fang, P. Chen, and G. Han, "Design and performance analysis of a new STBC-MIMO LoRa system," *IEEE Trans. Commun.*, vol. 69, no. 9, pp. 5744–5757, Sep. 2021.

[36] L. Li, M. C. Vuran, and I. F. Akyildiz, "Characteristics of underground channel for wireless underground sensor networks," in *Proc. 6th Annu. Medit. Ad Hoc Netw. Workshop (Med-Hoc-Net)*, Jun. 2007, pp. 13–15.

[37] M. Dobson, F. Ulaby, M. Hallikainen, and M. El-rayes, "Microwave dielectric behavior of wet soil—Part II: Dielectric mixing models," *IEEE Trans. Geosci. Remote Sens.*, vol. GE-23, no. 1, pp. 35–46, Jan. 1985.

[38] M. C. Vuran and I. F. Akyildiz, "Channel model and analysis for wireless underground sensor networks in soil medium," *Phys. Commun.*, vol. 3, no. 4, pp. 245–254, Dec. 2010.

[39] C. F. Dias, E. R. de Lima, and G. Fraidenraich, "Bit error rate closed-form expressions for LoRa systems under Nakagami and rice fading channels," *Sensors*, vol. 19, no. 20, pp. 1–11, Oct. 2019.

[40] A. Goldsmith, *Wireless Communications*. Cambridge, U.K.: Cambridge Univ. Press, 2005.

[41] T. K. Nguyen, H. H. Nguyen, and E. Bedeer, "Performance improvement of LoRa modulation with signal combining and semi-coherent detection," *IEEE Commun. Lett.*, vol. 25, no. 9, pp. 2889–2893, Sep. 2021.

[42] W. Foy, "Position-location solutions by Taylor-series estimation," *IEEE Trans. Aerosp. Electron. Syst.*, vol. AES-12, no. 2, pp. 187–194, Mar. 1976.

[43] B. Al Homssi, K. Dakic, S. Maselli, H. Wolf, S. Kandeepan, and A. Al-Hourani, "IoT network design using open-source LoRa coverage emulator," *IEEE Access*, vol. 9, pp. 53636–53646, 2021.